Transparent and flexible humidity sensor based on graphene oxide thin films prepared by electrostatic spray deposition technique

P. Songkeaw[1] · K. Onlaor[1] · T. Thiwawong[1] · B. Tunhoo[1]

Abstract

In this work, transparent and flexible humidity sensors based on graphene oxide film were prepared using the electrostatic spray deposition technique. Graphene oxide (GO) powder was synthesized using the modified Hummer's method, which was used as a precursor for thin-film deposition. The properties of GO films were characterized by X-ray diffraction, field-emission scanning electron microscope, Raman spectroscopy, Fourier transform infrared spectroscopy, and UV–Vis spectrophotometer. The effect of substrate temperature on the sensor properties was observed. The impedance of the device exhibited a lower value when increasing the relative humidity level. In addition, the device showed high sensitivity of more than 1117.3, fast response with 5 s, more than 60% optical transparency, and flexible property more than 2000 cycles. In addition, the equivalent circuit models of the devices were evaluated from complex impedance measurements used to explain the sensing mechanisms of the device.

1 Introduction

Humidity plays an important parameter in many fields of application and industries such as agriculture, pharmaceutical, and electronics [1]. Typically, the measurement and control of humidity value will be a factor in the manufacturing process in such industries. The humidity response of a device is mainly due to changes in the electrical properties of the sensing material when the amount of moisture or water molecule content around the device changes. Normally, the materials used to fabricate humidity devices include silicon, ceramic, semiconductor nanoparticles, metal oxide, and carbon-based materials [2]. Among these materials, carbon-based material possesses more advantages such as low cost and flexibility. Generally, there are many carbon-based structures used in the construction of humidity sensors, such as fullerene, nanotube, graphene, and graphite. One of those

materials is graphene oxide (GO), which exhibits high sensitivity for humidity measurement [3, 4].

GO is a one-family group of graphene material composed of graphene layers attached to functional groups. Therefore, the properties of GO are somewhat different from graphene materials, such as low electrical conductivity and optical property [5]. Moreover, GO has many functional groups from the oxidation reaction, meaning it has more hydrophilic properties [6]. The hydrophilic behavior of GO shows good sensitivity in absorbing water and moisture molecules. Typically, GO can be synthesized by the oxidation process between graphite and various acids [7]. However, Hummer's method [8] can be used to synthesize GO with more safety and high yield product. The product of the Hummer's method is in the form of GO powder, which can be dispersed in various solvents such as alcohol or organic solvents [9]. In the past, the process used to prepare a thin film of GO was based on a solution process such as spin-coating, drop-casting, and filtering [10, 11], which made it difficult to control the thickness of the produced films.

The electrostatic spray deposition (ESD) technique is a simple process for thin-film preparation. Normally, nanostructure thin films such as metal, metal oxide, and polymer [12–15] can be prepared by this method. In this technique, the precursor solution is fed through a metal nozzle. A syringe pump can control the solution flow rate. A finely charged droplet of precursor is generated by applying high DC voltage between

✉ T. Thiwawong
 thutiyaporn.th@gmail.com

[1] Electronics and Control Systems for Nanodevices Research Laboratory, College of Nanotechnology, King Mongkut's Institute of Technology Ladkrabang, Bangkok 10520, Thailand

the nozzle and substrate holder. The properties of the deposited film are dependent on the deposition parameters such as substrate temperature and deposition times. In addition, the ESD technique uses a scalability system to prepare large-area films with more advantages such as low-temperature deposition, operation at ambient atmosphere, and repeatability [14]. In other reports, the ESD technique was used to prepare GO or reduced GO thin films for various applications such as super hydrophilic surfaces and energy storage. [16, 17]. Furthermore, many reports have confirmed their ESD technique in practical electronic applications. Joshi et al. [18] reported on graphene films decorated with bimetallic Zn-Fe oxide for lithium-ion battery anodes. The precursor solutions were sprayed on stainless steel at the substrate temperature of 150 °C, while the battery properties were indicative of significantly improved lithium storage. In addition, highly conductive graphene paper was successfully fabricated on the nanofiber film/aluminum foil double-layer substrate by Yan et al. [19] and can be used in supercapacitors.

As mentioned above, among the applications that can be fabricated by the ESD technique, the humidity sensor has been widely studied, and has potential applications in many fields. Zeeshan Yousaf et al. [20] used MoS_2 as the humidity-sensing active layer on a glass substrate, and the relative humidity was presented in terms of resistance. The modified surface morphology of poly-vinyl alcohol (PVA) films using the ESD technique was fabricated by Ahmad et al. [21] and the relative humidity was also presented in terms of resistance. Although humidity sensor devices have been widely studied, they are restricted in properties of flexibility and transparency. The flexible and transparent humidity sensor has potential applications in many fields such as stretchable electronic devices for the agricultural and pharmaceutical sectors, and in wearable devices. To the best of our knowledge, there have been few reports on flexible and fully transparent humidity sensor devices based on GO film prepared by the ESD method.

In this work, GO thin film was prepared by the electrostatic spray deposition technique on a flexible and transparent plastic substrate. The effects of substrate temperature during the deposition process on the properties of graphene oxide film and the properties of fabricated humidity devices were investigated. In addition, the impedance analysis, equivalent circuits, flexible and transparent abilities of the devices were also reported.

2 Experimental

2.1 Materials preparation

Graphite oxide powder was prepared using the modified Hummer's method [8]. First, 1 g of graphite powder (Arcos Organics, USA) was mixed with 1 g of $NaNO_3$ and 46 ml of H_2SO_4 in an ice bath to prevent the explosion process. Then, 6 g of $KMnO_4$ was slowly added into the mixture solution, after which it was removed from the ice bath. The solution was stirred at room temperature for 1 h. For the oxidizing process, 70 ml of distilled water was slowly added to the mixture solution at a solution temperature of 90 °C for 2 h. After that, the mixture turned to bright yellow, after which 100 ml of distilled water was added, followed by 30 ml of H_2O_2 to stop the reaction process. The mixture solution was stirred for 20 min. After that, the solution was centrifuged at 6000 rpm for 10 min to harvest residue particles. Next, the particles were washed by DI water several times and dried at 120 °C to collect graphite oxide powder. Graphite oxide was re-dispersed in methanol solvent at a concentration of 0.2 mg/ml. Finally, the graphite oxide solution was sonicated for 1 h to exfoliate graphite oxide to GO. This solution was used as a precursor solution in the ESD process to prepare GO films.

2.2 Humidity sensor device fabrication

The transparent electrode of indium tin oxide (ITO) film on polyethylene naphthalate (PEN) substrate (Peccell Technologues, Inc.) was used as an electrode. Initially, the ITO electrode was masked with parallel line patterns and chemical etching with aqua regia solution for 10 min. The spacing gap between both planar ITO electrodes was 1 mm. Next, the substrate was cleaned using an alcohol process with soaking in a sonication bath following 15 min each for DI water, methanol, and isopropanol, respectively. The electrostatic spray deposition system was applied to prepare GO films. In this work, a syringe pump was fed precursor solution of the GO solution through a metal nozzle with a diameter of 0.1 mm. DC voltage was applied between the metal nozzle and substrate holder in order to disperse the liquid solution into small droplets that formed the GO film on the substrate. In the ESD experiment, 9 kV DC voltage was applied between the nozzle and substrate. The precursor flow rate and distance between the nozzle and substrate were fixed at 3 ml/h and 4 cm, respectively. To fabricate the flexible and transparent device, the thermal properties of PEN plastic exhibit the glass-transition temperature (Tg) at 120 °C. Moreover, the upper processing temperature of the PEN substrate for flexible electronics applications was found at temperatures below Tg [22]. In addition, the boiling point of methanol is about 64.7 °C. Therefore, the substrate temperatures of RT, 60 °C, and 80 °C were used to fabricate the flexible humidity sensor device. The substrate temperatures at room temperature (RT), 60, and 80 °C were controlled by a temperature controller, while deposition time was fixed at 45 min. The completed device had an active area of about 20×20 mm^2.

The physical properties of GO films were characterized by X-ray diffraction (XRD: D8 Discover) with X-ray source wavelength of 1.5418 Å, Raman spectroscopy (DXR smart Raman), field-emission scanning electron microscope (FE-SEM: JSM-7001F), UV–visible spectrophotometer (UV–Vis: Thermoelectron), and Fourier transform infrared spectroscopy (FTIR: PerkinElmer) to explain the structural, morphology, and optical properties.

The humidity response of the device was measured at various control humidity values that can be achieved with saturated salt solutions by using saturated aqueous solvents of LiCl, CH_3COOK, $MgCl_2$, $Mg(NO_3)_2$, NaCl, KCl, and KNO_3 for relative humidity values of 11, 23, 32, 52, 75, 84, and 93%RH, respectively [15]. A precision LCR meter (Agilent: E4980A) was used to record the impedance values at room temperature. To perform the flexibility measurement, the device was measured under bending conditions at various bending radii. Moreover, the endurance of the device after the bending cycles was demonstrated.

3 Results and discussion

Figure 1 shows the optical transmittance spectra of GO films prepared at RT, which was measured by UV–visible spectrophotometer in transmittance mode. The optical transmittance of the devices showed more than 60% in the visible region at a wavelength range of 400 to 800 nm. Typically, the optical properties of GO films depend on the physical properties of GO films, such as the thickness and reduction of GO [23]. The insets of Fig. 1 show the schematics for the GO device prepared by the ESD technique and a photograph of the fabricated device.

The XRD characteristics of the film can be used to perform the structural parameters such as d-spacing value, which was affected by the behavior properties of the deposited film. The diffraction patterns of GO films prepared at different substrate temperatures are shown in Fig. 2a. The results show that the dominant diffraction peak occurred at about 10.6°, which corresponds to (001) plane of GO [24]. While a broad peak at about 25° was observed, which is related to the amorphous-like carbon, including the impurities in the (002) plane of graphene film.[25]. Moreover, the diffraction peak occurred at 10.6° due to the effect of the functional group attached to the graphene layer, which expanded the spacing between the layers of graphene flakes. When depositing the film over a long time, the intensity of diffraction peaks also tends to be higher because of the more stacking of flakes of GO on the film, as shown in Fig. S1 of the supporting information. From the XRD pattern with various substrate temperatures, the XRD peaks exhibited lower intensity when the GO films were prepared at higher substrate temperatures, which results from the effect
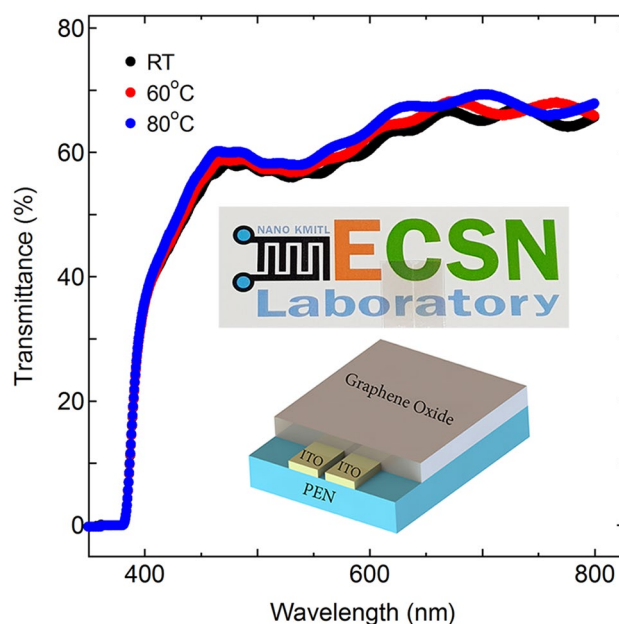

Fig. 1 Transmittance spectra of GO films prepared at different substrate temperatures (insets show a photograph and schematic structure of the fabricated humidity sensor device)

of higher solvent evaporation damage on the GO stacking layer. In addition, the number of layers (N) in GO flake can be performed from XRD peaks following Scherer's equation and Bragg's equation [26, 27]:

$$N = \frac{k\lambda}{d_{001}\beta\cos\theta} + 1, \tag{1}$$

where N is the number of GO layers, $k = 0.94$ is the shape factor, λ is a wavelength of the X-ray source, d_{001} is d-spacing of GO layer, β is the full width half maximum, and θ is the angle between the incident X-ray beam and scattering plane. Table 1 shows the structure parameter values of GO films prepared at various temperatures. The films prepared at RT exhibited the highest number of GO layers. The changing of structural properties in the film might be due to the vaporization of the intercalation vapor in the GO sheet during the deposition process [28].

The Raman characteristics of GO material can reveal the structural properties of the films. The Raman spectra exhibited three-band such as D peak at 1300 cm^{-1} (defected in the film), G peak at 1600 cm^{-1} that is the main peak for carbon material due to C–C or C=C bonding, and 2D peak at 2700 cm^{-1}, which is harmonic of G peak. The Raman spectra of the film prepared at various substrate temperatures are shown in Fig. 2b. The Raman peaks in the D–G band region (850–2000 cm^{-1}) were de-convoluted into eight components. These components can be defined as D*, D, D", D', D'+D³, D'+D⁴, and G peaks at wavenumbers of

1140, 1350, 1480, 1620, 1730, 1830, and 1580 cm^{-1}, respectively [29]. Moreover, two components at the 2D band in the region of 2500–3100 cm^{-1} were de-convoluted to $2D_1$ at 2700 cm^{-1}, and $2D_2$ at 2900 cm^{-1}, as shown in Fig. S3 of the supporting information.

From the de-convolution results of the Raman spectra, Table 1 shows the effect of substrate temperature on the ratio of D/G and 2D/G peaks. In other reports, the ratio of the intensity of D/G peaks corresponded to the degree of defects in the graphene sheet [30] and related to the inverse of crystal size on the basal plane in the GO film [28]. Thus, the increase of I_D/I_G ratio corresponded with increased defects in the prepared GO films. Typically, the ratio of I_D/I_G corresponds to the defects in graphene or graphene oxide films, in which these values are associated with the device sensitivity response properties. When comparing between graphene and graphene oxide with increased defects, the graphene oxide film will have a better sensitivity response [31–34]. Also, the characteristics of layers in graphene flake can be performed with the ratio of I_{2D}/I_G peaks. Therefore, the changes in characteristics of the GO film at various substrate temperatures resulted from the effect of the reaction of the solvent and the functional groups in the GO sheet. This feature is found in GO and reduced GO films that are annealed at low temperatures [35].

FTIR transmittance spectra of the film prepared at various substrate temperatures are shown in Fig. 2c. The results exhibited more detail about the functional group in the film. Typically, a broad spectrum at a wavenumber region of about 3000–3700 cm^{-1} was observed due to the overlapping of O–H stretching for moisture molecule, hydroxyl, and carboxyl groups [36]. The strong peak at 1627 cm^{-1} is a characteristic of the C=C bond in the polycyclic aromatic ring of the graphene structure [37]. Moreover, the peaks at a wavenumber of 2924, 1726, and 1409 cm^{-1} are defined as C–H, C=O, and C–O, respectively [38]. The C–O and C=O absorption peaks decreased with increasing substrate temperature.

The surface morphology of the GO films was obtained by FE-SEM measurement. Figure 3a–c exhibits the surface morphology of the film. The morphology of the film prepared at RT exhibited small grains, whereas the surface morphology for the film prepared at high substrate temperature showed large grains with discontinuous surfaces due to the effect of higher solvent evaporation during film deposition. The insets of Fig. 3 show high-magnification images of the morphology. The surface morphology of the films depicts the stacking of nanosheets with network structures of wrinkled GO flakes. Normally, a slow rate of solvent evaporation was observed at the low-temperature deposit that precursor
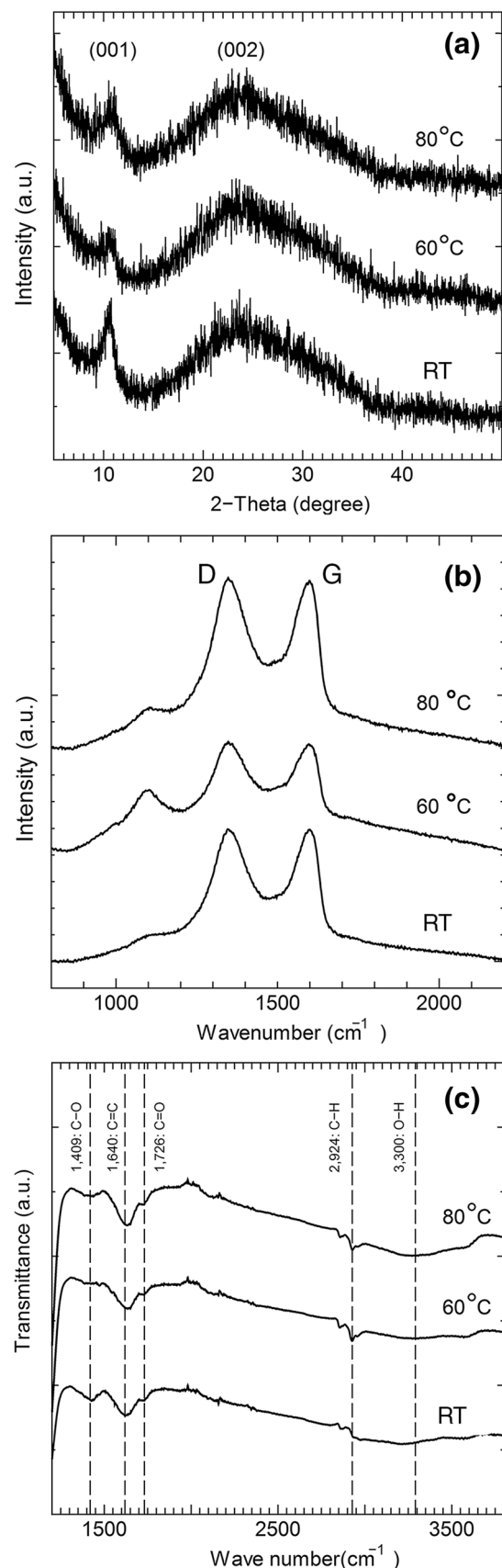
Table 1 The structural parameters from X-ray diffraction and Raman spectroscopy of GO films prepared at different substrate temperatures

Substrate temperature	2θ (degree) at (001) plane	FWHM	Layer	I_D/I_G	I_{2D}/I_G
RT	10.66	1.88	5.06	1.59	0.15
60	10.56	3.45	2.70	1.70	0.11
80	10.64	2.68	3.54	1.63	0.14

droplet has been dropped and slowly spread to form the film on the substrate. Contrarily, a fast rate of solvent evaporation was found when depositing film at a high substrate temperature. The droplets gather together with neighboring droplets to form larger grains on the surface of the film. The thicknesses of deposited GO films were evaluated by estimating from ten points of the cross-section image of the films, as shown in Fig. S4 of the supporting information. The thickness of the films at substrate temperatures of RT, 60, and 80 °C was about 254.3 ± 20.4, 168.6 ± 16.7, 220 ± 35.6 nm, respectively. The thickness of the GO films changed when preparing the film at a temperature higher than the boiling point of methanol solvent due to the influence of forming functional groups in the GO layer.

The humidity response of the device prepared at various substrate temperatures is shown in Fig. 4a. The results exhibited the relation between relative humidity and the impedance of the device. The sensitivity (S) of the sensor device was estimated from the following equation [39, 40]:

$$S = \frac{Z_L}{Z_H}, \tag{2}$$

where Z_L and Z_H denote the impedances of the device under relatively low and high humidity conditions. The maximum sensitivity (S) of the device was about 1117.3, 122.8, and 66.9 in the range of 11–93%RH, for GO device prepared at substrate temperatures of RT, 60 and 80 °C, respectively. From the results, the impedance of the device decreases, while the relative humidity increases due to the effect of the free transfer of ions on the moisture layer in GO film [41], the intercalation of water molecules into gaps between GO layers [4], and the effect of the GO structure [42–46]. The highest humidity sensitivity response of the device was found at RT, which corresponds to the highest number of GO layers evaluated from the XRD results. Also, the device prepared at RT substrate temperature was tested with various gases of methanol, ethanol, acetone, and isopropanol with a fixed concentration of 5000 ppm [47]. The sensitivity response of the device is shown in Fig. 4b. The results confirmed that the humidity response of the device has dominant characteristics. From the results, the film prepared at room temperature exhibits the maximum humidity sensitivity
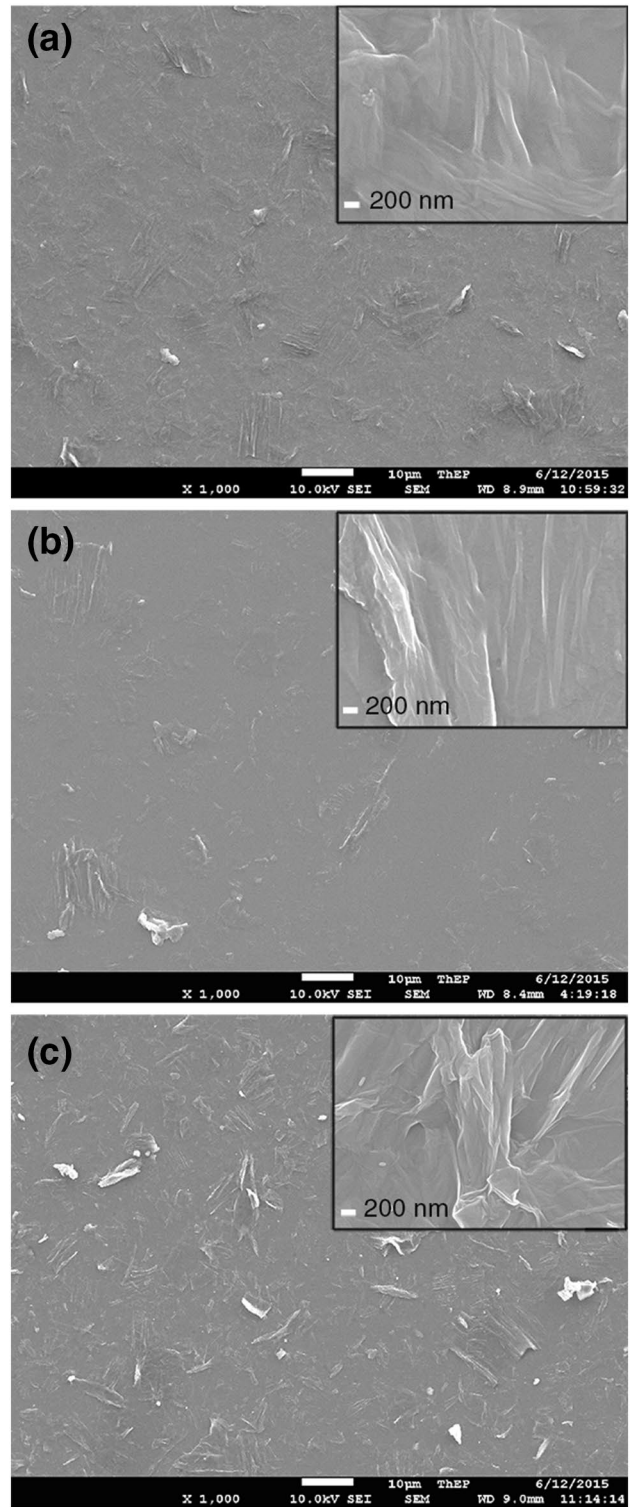
Fig. 3 **a-c** Surface morphology of GO films prepared at different substrate temperatures **a** RT, **b** 60, and **c** 80 °C. Inset: 30,000 times magnification
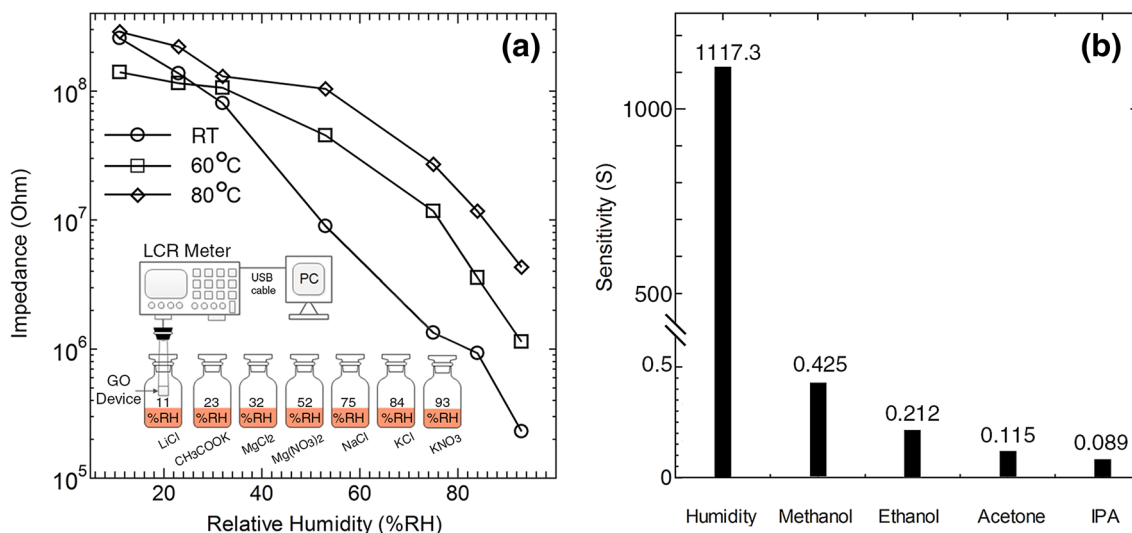
Fig. 4 **a** Humidity response of the prepared device at different substrate temperatures; the inset shows a humidity-sensing setup block diagram and **b** comparison of humidity and gas sensitivities from the device prepared at RT

response, in spite of it having the lowest I_D/I_G. Therefore, the defect does not dominate the main sensitivity response mechanism of the device. One of the mechanisms that can be explained is the hopping of ions between hydroxyl functional groups [34], which will be discuss later.

Moreover, the characteristics of the device were tested, such as cyclic response and hysteresis errors. A hysteresis error is a performance parameter of a humidity sensor, the shift of sensor output between the absorption and desorption process. The device deposited at the substrate temperature of RT was measured at humidity levels from 11%RH to

93%RH for absorption process and re-measured at humidity levels from 93%RH to 11%RH for the desorption process, as shown in Fig. 5a. The results can be calculated to a hysteresis error (γ_H) [15], which found maximum error at ±1.27% at a humidity level of 84%RH. Normally, a hysteresis error in a humidity sensor device comes from imbalance in the moisture molecule absorption and desorption process during measurement.

To identify the response and recovery properties of the device, the optimized device was measured at 11%RH, then changed to 93%RH for 200 s and returned to 11%RH.
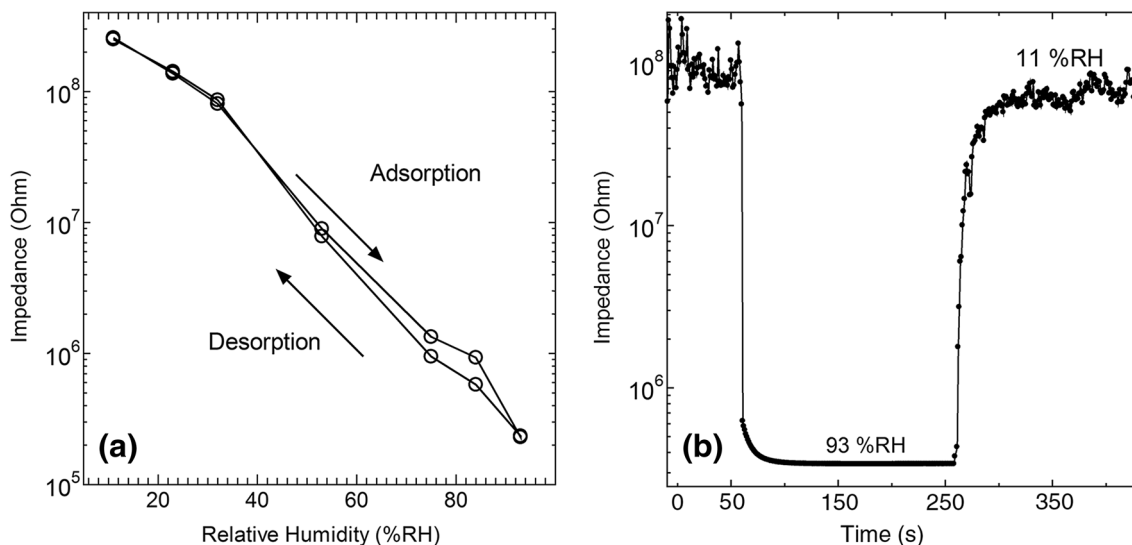

Fig. 5 **a** Hysteresis characteristic and **b** cyclic response between 11 and 93%RH of the sensor device with GO films prepared at the substrate temperature of RT

The results of the recovery properties are shown in Fig. 5b. The response and recovery times for this GO device were about 5 and 11 s, respectively. These results also showed rapid responses compared to other works [46]. The fast responses result from the high d-spacing in GO flake where the water molecules were easily diffused and removed into the intercalation layer of GO during measurement.

The flexibility of the device was demonstrated. The device was tested at an unbending condition called "flat condition". After that, the device was measured under bending conditions at various bending radii, as shown in Fig. 6a. Comparisons of humidity response were shown in terms of normalized sensitivity following the relation below:

$$\text{Normalized sensitivity} = \frac{S_{\text{bend}}}{S_{\text{flat}}}, \tag{3}$$

where S_{flat} is the humidity sensitivity of the device at flat condition, and S_{bend} is the humidity sensitivity of the device under bending conditions.

The device exhibited a sensing response drop to 80% of the flat condition at a bending radius of 10 mm, which indicated the device could be used in flexible sensor applications. Moreover, the endurance of the bending test with bending cycles was recorded by computer control with a motorized moving stage. The normalized sensitivity of the device after bending cycles is shown in Fig. 6b. After measurement up to 2000 cycles, the device still exhibited a sensitivity value of more than 75% of the initial condition. The inset of Fig. 6b shows the movable stage for bending measurement in the cyclic endurance test.

To test the sensing mechanism from the equivalent circuit models of the GO humidity sensor [44], the impedances of the device were measured at various frequency responses in each humidity level of 11, 23, 32, 52, 75, 84, and 93%RH, respectively. An AC signal (1 V amplitude, frequency range from 20 Hz to 2 MHz) was applied to assess the impedance characteristics of the device. The relation between the real part and imaginary part of the impedance output of the device or Cole–Cole plot was obtained at various humidity values, as shown in Fig. 7. From the results, semicircles were observed in decreasing size when the humidity levels increased. In the case of humidity value of 93%RH, the Cole–Cole plot exhibits a semicircle shape comprising a linear tail. That linear tail in the Cole–Cole plot occurred in low-frequency measurement [45].

Typically, there are several types of equivalent circuit used to explain the mechanisms in the electrochemical process [45]. The basic circuit for low humidity levels is composed of resistance and capacitance components. In the case of a semicircle graph of the Cole–Cole plot, the prediction equivalent circuit of a sensing mechanism is shown in the inset (a) of Fig. 7, while the resistance and capacitance of the device are defined as R_{p} and C_{p}, respectively. R_{s} is the contact resistance of the GO film. In the region of low humidity value, the moisture molecule was adsorbed of GO films which physisorption process with hydrogen bonds between oxygen atoms of GO and hydrogen atom of moisture molecule or hydrogen atom of function group of GO and oxygen atom of moisture molecule to stack layer of water. The interaction between moisture molecules and sensing layer in the device might affect a reduction in the size of the semicircle graph when the humidity levels are increased.
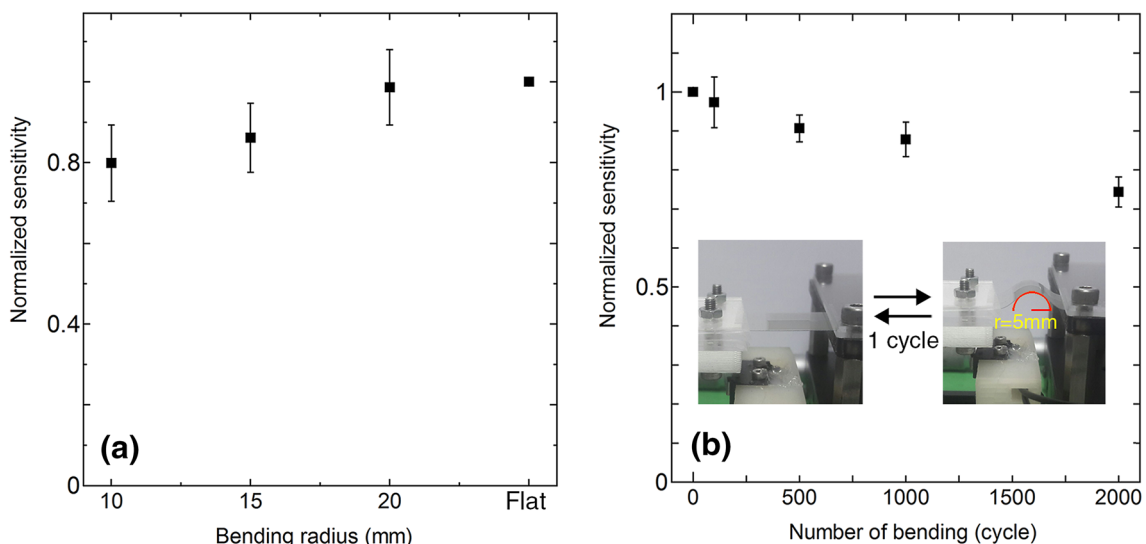

Fig. 6 **a** Normalization sensitivity of the device under bending conditions and **b** normalization sensitivity of the device after the bending cycle test
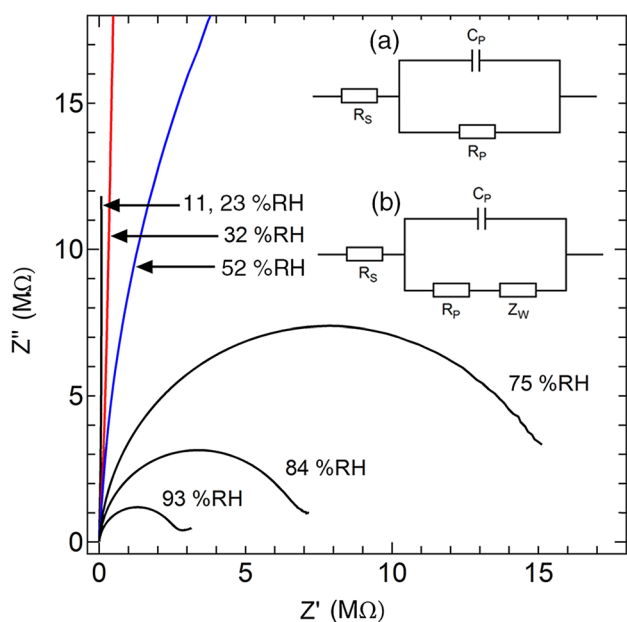
Fig. 7 Cole–Cole plot of GO device prepared at RT. Inset: equivalent circuits of the device

The combination of the resistances and capacitances of the sensing layer, as well as the effect of ion diffusion and charge transfer characteristics, will change the electrical conductivity of the device when changing the humidity levels. Prior to the adsorption of water, moisture ions (H_3O^+) on the GO surface were conducted with the hopping of ion between hydroxyl functional groups of graphene oxide. Then, the water adsorption makes the ions hop easily between closer moisture molecules. Therefore, the impedance of GO decreased when humidity levels changed to a higher value [45]. In addition, Guo et al. [48] reported the interactions between moisture molecules and oxygen functional groups on the graphene surface by the density functional theory (DFT). They demonstrated that the hydroxyl groups play a role in absorbing moisture molecules more than the epoxy groups, which corresponded to the results of the FTIR spectra.

In the case of the highest humidity level of 93%RH, the equivalent circuit is shown in the inset (b) of Fig. 7. The special component of the Warburg element (Z_W) was added into the circuit with serried to R_p of the device. The Cole–Cole plot exhibited a semicircle shape with a linear tail that has an equivalent mechanism. In this case, the charge in transport mechanisms depends on the moisture molecules, which can be explained by Grotthus' chain reaction [45]. When the moisture content is higher, the hydrolysis process of functional groups in the film occurs, and the size of the semicircle comprises a linear tail. At this point, the Warburg element was added to the equivalent model due to the effect of moisture molecules intercalated into the GO layer in the film. These intercalations make the films exhibit lower conductivity.

A comparison of other reports on the properties of humidity sensors is shown in Table 2. The humidity sensor device fabricated by the ESD technique exhibited high sensitivity. Moreover, the device can be used for flexible and transparent electronics applications.

4 Conclusion

GO films were prepared by electrostatic spray deposition on a flexible substrate at various substrate temperatures for humidity sensor applications. This technique can be used to fabricate humidity sensor devices with facile repeatability and scalability. The fabricated device exhibited high sensitivity, fast response, and high optical transmittance. The device exhibited maximum sensitivity (S) of 1117.3 in the range of 11 to 93%RH. Response time and recovery time for this GO device were about 5 and 11 s for humidity adsorption from 11 to 93%RH and humidity desorption from 11 to 93%RH, respectively. The maximum value of hysteresis error was found at $\pm\,1.27\%$, at a humidity level of 84%RH. Moreover, the complex impedance measurement at various humidity levels was used to analyze the mechanisms of the GO device, which comprised physisorption and chemisorption mechanisms.

Table 2 Example comparison of humidity sensors

Sensing layer (technique)	Type of sensing response	Sensitivity (formula)	Response/ recovery times (s)	Flexibility	Transparency	Refs
Graphene (CVD)	Resistance	0.31%/%RH ($\Delta R/R/\%$RH)	0.6/0.4	Cannot bend	Opaque	[49]
Graphene/TiO$_2$ (sol–gel)	Impedance	151 (Z_L/Z_H)	128/68	Cannot bend	Opaque	[50]
Graphene/methyl-red (printing)	Resistance	96.36% (($\Delta R/R$)$\times$100)	0.25/0.35	Can be bent	80%	[51]
Partially rGO (drop-casting)	Resistance	105% (($\Delta R/R$)$\times$100)	4.2/3.6	Can be bent	Opaque	[52]
Partially rGO (dried foam)	Impedance	33.254% (($\Delta Z/Z$)$\times$100)	50/79	Can be bent	80%	[46]
GO (ESD)	Impedance	1117.3 (Z_L/Z_H)	5/11	Can be bent	60%	This work

References

1. G. Naik, S. Krishnaswamy, Room-temperature humidity sensing using graphene oxide thin films. Graphene **05**, 1–13 (2016)
2. H. Farahani, R. Wagiran, N.M. Hamidon, Humidity sensors principle, mechanism, and fabrication technologies: a comprehensive review. Sensors **14**, 2014 (2014)
3. S. Borini et al., Ultrafast graphene oxide humidity sensors. ACS Nano **7**, 11166–11173 (2013)
4. H. Bi et al., Ultrahigh humidity sensitivity of graphene oxide. Sci. Rep. **3**, 2714 (2013)
5. S. Park, R.S. Ruoff, Chemical methods for the production of graphenes. Nat. Nanotechnol. **4**, 217 (2009)
6. W.-P. Chen, Z.-G. Zhao, X.-W. Liu, Z.-X. Zhang, C.-G. Suo, A capacitive humidity sensor based on multi-wall carbon nanotubes (MWCNTs). Sensors **9**, 2009 (2009)
7. D.C. Marcano et al., Improved synthesis of graphene oxide. ACS Nano **4**, 4806–4814 (2010)
8. D.R. Dreyer, S. Park, C.W. Bielawski, R.S. Ruoff, The chemistry of graphene oxide. Chem. Soc. Rev. **39**, 228–240 (2010)
9. M.F. Craciun, I. Khrapach, M.D. Barnes, S. Russo, Properties and applications of chemically functionalized graphene. J. Phys. Condens. Matter **25**, 423201 (2013)
10. J. Gascho, S. Da Costa, A. Recco, S. Pezzin, Graphene oxide films obtained by vacuum filtration: x-ray diffraction evidence of crystalline reorganization. J. Nanomater. **2019**, 1–12 (2019)
11. I. Karteri, S. Karatas, M. Cavas, B. Arif, F. Yakuphanoglu, The dielectric and optoelectronic properties of graphene oxide films by solution-casting technique. J. Nanoelectron. Optoelectron. **11**, 29 (2015)
12. I.B. Rietveld, K. Kobayashi, H. Yamada, K. Matsushige, Process parameters for fast production of ultra-thin polymer film with electrospray deposition under ambient conditions. J. Colloid Interface Sci. **339**, 481–488 (2009)
13. A. Jaworek, Electrospray droplet sources for thin film deposition. J. Mater. Sci. **42**, 2007 (2007)
14. A. Jaworek, A. Sobczyk, A. Krupa, M. Lackowski, T. Czech, Electrostatic deposition of nanothin films on metal substrate. Bull. Pol. Acad. Sci. **57**, 63 (2009)
15. T. Thiwawong, K. Onlaor, B. Tunhoo, A humidity sensor based on silver nanoparticles thin film prepared by electrostatic spray deposition process. Adv. Mater. Sci. Eng. **2013**, 7 (2013)
16. E. Adelowo, A.R. Baboukani, C. Chen, C. Wang, Electrostatically sprayed reduced graphene oxide-carbon nanotubes electrodes for lithium-ion capacitors. J. Carbon Res. **4**, 31 (2018)
17. L.-J. Wang et al., Large-area graphene coating via superhydrophilic-assisted electro-hydrodynamic spraying deposition. Carbon N. Y. **79**, 294–301 (2014)
18. B. Joshi et al., Electrosprayed graphene films decorated with bimetallic (zinc-iron) oxide for lithium-ion battery anodes. J. Alloys Compd. **782**, 699–708 (2019)
19. J.-X. Yan et al., Highly conductive graphene paper with vertically aligned reduced graphene oxide sheets fabricated by improved electrospray deposition technique. ACS Appl. Mater. Interfaces **11**, 10810–10817 (2019)
20. H.M.Z. Yousaf, S.W. Kim, G. Hassan, K. Karimov, K.H. Choi, M. Sajid, Highly sensitive wide range linear integrated temperature compensated humidity sensors fabricated using electrohydrodynamic printing and electrospray deposition. Sens. Actuators B Chem. (2020). https://doi.org/10.1016/j.snb.2020.127680
21. Z. Ahmad, M. Abbas, I. Gunawan, R.A. Shakoor, F. Ubaid, F. Touati, Electro-sprayed PVA coating with texture-enriched surface morphology for augmented humidity sensing. Prog. Org. Coat. **117**, 7–9 (2018)
22. W. Macdonald et al., Latest advances in substrates for flexible electronics. J. Soc. Inf. Disp. **15**, 1075–1083 (2007)
23. P. Gangwar, S. Singh, N. Khare, Study of optical properties of graphene oxide and its derivatives using spectroscopic ellipsometry. Appl. Phys. A **124**, 620 (2018)
24. F.T. Johra, J.-W. Lee, W.-G. Jung, Facile and safe graphene preparation on solution based platform. J. Ind. Eng. Chem. **20**, 2883–2887 (2014)
25. T.F. Tefo et al., Synthesis and characterization of graphene thin films via Hummer's method. Nanotechnology **1**, 2012 (2012)
26. B.K. Saikia, R.K. Boruah, P.K. Gogoi, A X-ray diffraction analysis on graphene layers of Assam coal. J. Chem. Sci. **121**, 103–106 (2009)
27. S. Venkatachalam et al., Characterization of vacuum-evaporated ZnSe thin films. Mater. Charact. **58**, 794–799 (2007)
28. S. You et al., Selective intercalation of graphite oxide by methanol in water/methanol mixtures. J. Phys. Chem. C **117**, 1963–1968 (2013)
29. S. Claramunt, A. Varea, D. López-Díaz, M.M. Velázquez, A. Cornet, A. Cirera, The importance of interbands on the interpretation of the Raman spectrum of graphene oxide. J. Phys. Chem. C **119**, 10123–10129 (2015)
30. E.-Y. Choi et al., Noncovalent functionalization of graphene with end-functional polymers. J. Mater. Chem. **20**, 1907–1912 (2010)
31. F. Ricciardella et al., Effects of graphene defects on gas sensing properties towards NO2 detection. Nanoscale **9**, 6085–6093 (2017)
32. J.T. Robinson, F.K. Perkins, E.S. Snow, Z. Wei, P.E. Sheehan, Reduced graphene oxide molecular sensors. Nano Lett. **8**, 3137–3140 (2008)
33. G. Lu et al., Toward practical gas sensing with highly reduced graphene oxide: a new signal processing method to circumvent run-to-run and device-to-device variations. ACS Nano **5**, 1154–1164 (2011)
34. S. Cui et al., Ultrasensitive chemical sensing through facile tuning defects and functional groups in reduced graphene oxide. Anal. Chem. **86**, 7516–7522 (2014)
35. A. Hussein, S. Sarkar, B. Kim, Low temperature reduction of graphene oxide using hot-plate for nanocomposites applications. J. Mater. Sci. Technol. **32**, 411–418 (2016)
36. M.K. Rabchinskii et al., Facile reduction of graphene oxide suspensions and films using glass wafers. Sci. Rep. **8**, 14154 (2018)
37. C. Valencia, H.C. Valencia, F. Zuluaga, E.M. Valencia, H.J. Mina, D.C. Grande-Tovar, Synthesis and application of Scaffolds of Chitosan-graphene oxide by the freeze-drying method for tissue regeneration. Molecules **23**, 2018 (2018)
38. B. Sudesh, N. Kumar, S. Das, C. Bernhard, G.D. Varma, Effect of graphene oxide doping on superconducting properties of bulk MgB2. Supercond. Sci. Technol. **26**, 95008 (2013)
39. L.D. Bharatula, M.B. Erande, I.S. Mulla, C.S. Rout, D.J. Late, SnS2 nanoflakes for efficient humidity and alcohol sensing at room temperature. RSC Adv. **6**, 105421–105427 (2016)
40. Y. Kumar, A. Sharma, P. Shirage, Shape-controlled CoFe 2 O 4 nanoparticles as an excellent material for humidity sensing. RSC Adv. **7**, 55778–55785 (2017)
41. Y. Yao, X. Chen, J. Zhu, B. Zeng, Z. Wu, X. Li, The effect of ambient humidity on the electrical properties of graphene oxide films. Nanoscale Res. Lett. **7**, 363 (2012)
42. A. Ghosh, D. Late, L. Panchakarla, A. Govindaraj, C. Rao, NO2 and humidity sensing characteristics of few-layer graphene. J. Exp. Nanosci. **4**, 313–322 (2009)

43. T.S. Sreeprasad et al., Electron-tunneling modulation in percolating network of graphene quantum dots: fabrication, phenomenological understanding, and humidity/pressure sensing applications. Nano Lett. **13**, 1757–1763 (2013)

44. K. Han et al., Material characteristics and equivalent circuit models of stacked graphene oxide for capacitive humidity sensors. AIP Adv. **6**, 35203 (2016)

45. A. Miyamoto et al., Solid electrolyte gas sensor based on a proton-conducting graphene oxide membrane. ACS Omega **2**, 2994–3001 (2017)

46. X. Feng, W. Chen, L. Yan, Free-standing dried foam films of graphene oxide for humidity sensing. Sens. Actuators B Chem. **215**, 316 (2015)

47. D. Zhang, A. Liu, H. Chang, B. Xia, Room-temperature high-performance acetone gas sensor based on hydrothermal synthesized SnO2-reduced graphene oxide hybrid composite. RSC Adv. **5**, 3016 (2014)

48. L. Guo et al., Two-beam-laser interference mediated reduction, patterning and nanostructuring of graphene oxide for the production of a flexible humidity sensing device. Carbon N. Y. **50**, 1667–1673 (2012)

49. A.D. Smith et al., Resistive graphene humidity sensors with rapid and direct electrical readout. Nanoscale **7**, 19099–19109 (2015)

50. W.-D. Lin, C.-T. Liao, T.-C. Chang, S.-H. Chen, R.-J. Wu, Humidity sensing properties of novel graphene/TiO2 composites by sol–gel process. Sens. Actuators B Chem. **209**, 555–561 (2015)

51. S. Ali, A. Hassan, G. Hassan, J. Bae, C.H. Lee, All-printed humidity sensor based on graphene/methyl-red composite with high sensitivity. Carbon N. Y. **105**, 23–32 (2016)

52. M. Shojaee, S. Nasresfahani, M.K. Dordane, M.H. Sheikhi, Fully integrated wearable humidity sensor based on hydrothermally synthesized partially reduced graphene oxide. Sens. Actuators A Phys. **279**, 448–456 (2018)